Type of the Paper (Article)

Experimental assessment of the spatial and temporal distribution of non-contact tonometer airflows

Daniela Oehring [1]*, David Jenkins [2], Phillip Buckhurst [1], Hetal Buckhurst [1]

[1] Faculty of Medicine, Dentistry and Human Sciences, University of Plymouth, Plymouth UK
[2] Faculty of Science and Engineering, School of Engineering, Computing and Mathematics, University of Plymouth, Plymouth UK
* Corresponding author

Abstract: (1) Aim of the study was to investigate the spatial and temporal characteristics of the airflow created by two commercially available non-contact tonometers, the CorvisST and the Ocular Response Analyser. (2) The airflow pressure was measured using a MEMS pressure sensor to investigate the spatial and temporal distribution. The airflow from the CorvisST and Ocular Response Analyser were mapped to a 600µm and a 1mm resolution grid, respectively. (3) Central airflow pressure of the CorvisST (96.4 ± 1.4)mmHg was higher than the Ocular Response Analyser (91.7 ± 0.7)mmHg. The duration of the air-puffs also differed, with the CorvisST showing a shorter duration (21.483 ± 0.2881)ms than the ORA (23.061 ± 0.1872)ms. The rising edge of the CorvisST airflow pressure profile demonstrated a lower gradient (+8.94mmHg/ms) compared to the Ocular Response Analyser (+11.00mmHg/ms). Both had similar decay response edges; CorvisST -11.18mmHg/ms, Ocular Response Analyser -11.65mmHg/ms. (4) The study presents a valid method to investigate physical dimensions of the airflow pressure of non-contact tonometers. Novel findings relating to the magnitude, duration and spatial characteristics of the respective airflow pressures are reported. It is anticipated that this information will better inform clinical studies and theoretical models relating to ocular biomechanics.

Keywords: Air puff, CorvisST, ORA, Airflow pressure of NCT, Physical dimension of jet stream, Temporal and spatial distribution of the air puff

Citation: Lastname, F.; Lastname, F.; Lastname, F. Title. *Appl. Sci.* **2021**, *11*, x. https://doi.org/10.3390/xxxxx

1. Introduction

Tonometers are used to measure the eye's intraocular pressure. Various different types of tonometric devices are available, but all are based on measuring the force needed to applanate or indent a given surface area of the cornea to infer the pressure within the eye. Non-contact tonometers that utilise an air-puff to applanate the cornea, have grown in popularity given that they are non-contact and require minimal training to operate. Limitations relating to the influence of corneal biomechanics on the intraocular pressure measurements are well-recognised with all tonometric tests. In an attempt to overcome some of these, non-contact tonometers such as the CorvisST (Oculus Optikgeräte GmbH; Wetzlar, Germany) and the Reichert Ocular Response Analysers (ORA; Reichert Technologies Inc., New York, USA) have been developed to provide simultaneous assessment of both corneal biomechanics and intraocular pressure. By combining non-contact tonometry with an ultra-high-speed Scheimpflug camera, the CorvisST captures the dynamic response of the cornea to the air-puff at 4330 frames per second. The device records the displacement of the corneal surface caused by the application of the airflow over time and derives the intraocular pressure by determining the time to first corneal applanation. [1] The biomechanical characteristics derived by the CorvisST are based on the corneal deformation response recorded with the inbuilt high-speed camera system. Similarly, the ORA provides a non-invasive measurement of intraocular pressure utilising an airflow of 300m/s for approximately 20ms to applanate the cornea. [2] Following a controlled increase in airflow pressure during the inward deformation of the cornea, a defined decrease in pressure occurs through the outward phase of the deformation. [2-5] During the measurement sequence, the ORA emits infrared light and detects the intensity of the light reflected from the cornea. The temporal distribution of the intensity of the infrared radiation results in two distinct maxima, denoting the first and second corneal applanation events. Through the use of this data and empirically derived algorithms, the device is able to offer measures of corneal hysteresis and corneal resistance factors that can be considered with the intraocular pressure measurements. [2]

Despite significant efforts to understand corneal biomechanics with the use of the CorvisST and ORA [6-16], there is a dearth of literature on the actual physical and geometric properties of the airflow pressure applied to the cornea with these devices. Indeed, the physical attributes of the air-pressure applied during non-contact tonometry is fundamental to the measures of both intraocular pressure and corneal biomechanics. [17] For both the CorvisST and ORA the airflow pressure for each tonometer measurement is generated by an inbuilt piston-cylinder system (further referred as chamber pressure), Figure 1. The temporal profile of the chamber pressure varies in shape, height and width depending on the specific tonometer. The tonometer nozzle consists of a tube with an inner diameter of approximately 1 to 2mm, through which, the airflow exits the device. Most tonometers require an 11mm distance between the nozzle and the eye. When considering the jet stream created by the tonometer, the nozzle-to-eye distance is likely to affect the cross-sectional profile of the pressure applied to the eye i.e. a long nozzle-to-eye distance is likely to result in a narrower cross-section of the airflow being applied at the corneal plane when compared to a short distance. This effect is likely to be pronounced as the velocity of the airflow is assumed to lie within a narrow range of 300 to 400km/h. [18, 19] Due to the nozzle-to-eye distance and subsequent change in the pressure profile, it may be justifiably assumed that the spatial and temporal profile of the actual airflow pressure on the cornea differs significantly from that of the piston chamber pressure. [19]

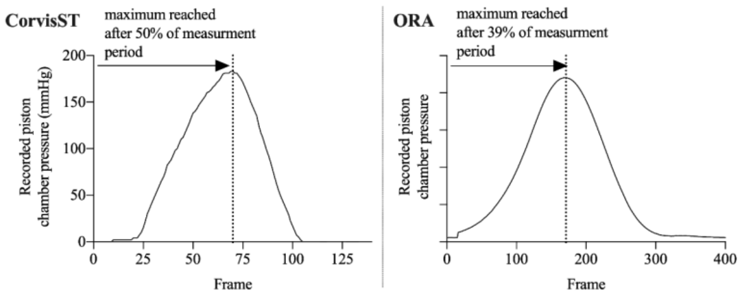

(a) (b)

Figure 1: Piston chamber pressure of non-contact air-puff tonometer devices. (a) The CorvisST provides piston chamber pressure values over a period of 140 frames (b) whilst the ORA provides this over 400 frames.

Through empirical assessments and numerical simulations, previous attempts to characterise the CorvisST airflow pressure at eye-to-nozzle working distances provide disparate results. [20-22] Using a differential pressure sensor, Kling et al. [22] demonstrated the CorvisST airflow on the corneal surface reached a maximum of 120mmHg lasting 27.50ms. Fitting the temporal pressure profile with a linear function, the study reported that the increasing pressure phase was maintained for 18.2ms whilst the decreasing phase only lasted for 9.3ms. In comparison, Metzler et al. [20, 23] used hot-wire anemometry at different sensor-to-nozzle distances to obtain measures of the CorvisST airflow velocity. Between 9mm and 12mm, the airflow velocity was above 90m/s whereas at the nozzle it was over 100m/s [20, 23]. With the use of Navier-Stokes equation the pressure at the nozzle and corneal plane (11mm distance) were estimated to be 100.9mmHg and 124.6mmHg, respectively. In a numerical simulation experiment, Bahr et al. [21] reported the maximal airflow velocity to be 80m/s at the nozzle, similar results to those reported by Metzler, but at the corneal surface they found the maximal airflow pressure to be significantly lower at approximately 2.3kPa (17.3mmHg) [21]. Despite these attempts to characterise the CorvisST airflow, there is still ambiguity surrounding its physical profile and in regard to the ORA, even little is known about the air flow's spatial and temporal distribution. Work by Luce [24], suggests that the air flow demonstrates a Gaussian profile with a constant width. According to the operation manual the shape of the pressure curve varies with the eye's intraocular pressure; the higher the intraocular pressure, the higher the amplitude of the pressure curve.

Given that assessment of the intraocular pressure and corneal biomechanics with the CorvisST and ORA are based upon the application of known forces to the cornea, as yet, there is no comprehensive evidence available about the dimension, magnitude and duration of the airflow pressure generated by these devices. Moreover, it is still unclear how much of the cornea is affected during application of the pressure and how repeatable the airflow pressure is across the entire ocular surface. Since the introduction of the ORA and CorvisST there has been much clinical interest in assessing corneal biomechanics in vivo and many have compared and contrasted the metrics produced by these two devices [25-28] but little consideration has been given to assessing whether the principal airflow used by the devices are equivalent or not. Thus, the principal aim of this experimental study was to develop a method to investigate the spatial and temporal characteristics of the airflow pressure produced by the CorvisST and ORA and assessing their concordance.

2. Materials and Methods

To investigate the airflow pressure of the CorvisST and ORA, a high precision sensor and recording system was developed capable of measuring low-level pressure of short duration. The investigation also assesses the utility of a novel mapping system that was designed and validated to assess the spatial and temporal characteristics of the airflow.

2.1 Experimental set up

2.1.1 Pressure sensor

For the purposes of the investigation, the geometric extent of the airflow was estimated to be analogous to the average corneal diameter size of 12mm and the typical non-contact tonometer operating distance was assumed to be 11mm. In view of these assumptions, a range of sensors where tested (silicon piezoresistive, dual pressure sensor; piezoresistive transducer, differential pressure sensor, piezoresistive static force sensor; piezoresistive transducer, gauge pressure sensor; differential compensated pressure sensor) for their applicability. The Linear-Time-Invariant systems were found to be best suited for the requirements and thus, the gauge pressure sensor (the MPX5050GP (Freescale Semiconductor, Inc.) was chosen for investigation. The MPX5050GP is a piezoresistive, monolithic silicon pressure sensor which offers a differential sensitivity of 7.241mmHg, for a full scale of 362.004mmHg with an accuracy of ±2.5% over the whole detection span.

2.1.2 Mapping procedure

Using a millimetre graph paper, the size of the area imaged by CorvisST at 11mm distance from the nozzle was determined to be (12.7 x 10.6) mm. The pressure sensor with a tube opening of 1.0mm diameter was placed 11mm from the CorvisST nozzle; the CorvisST screen was captured with a conventional digital camera. The image of the sensor tube opening on the CorvisST screen was used to develop a mapping grid (Figure 2a) which was the size of the CorvisST screen (75 x 90)mm. Since the CorvisST screen is tetragon shaped, the trace of the sensor tube opening was initially centralised within the tetragon and replicated; then subsequently placed along the x and y axis to fill the area of the grid. Using this procedure, the grid was comprised of 137 measurement points, 12 to 13 horizontally and 11 vertically. The mapping grid was used to measure the absolute pressure of the CorvisST airflow. For assessing the spatial extent of the airflow pressure, the

Preprints (www.preprints.org) | NOT PEER-REVIEWED | Posted: 27 January 2021 doi:10.20944/preprints202101.0566.v1

resolution of the measurement map was increased by using an aluminium aperture, fixed at the pressure sensor tube opening (Figure 2b). Initial test measurements demonstrated that optimal resolution could be reached with an aperture diameter of 600µm. Measurement of the pressure was dependent upon the diameter of the tube opening; small aperture size was found to decrease the output signal. When using an aperture diameter smaller than 600µm, it was not possible to differentiate the magnitude of the output signal from the sensor noise. Using the 600µm aperture the second mapping grid was created with 382 measurement points, Figure 2. This mapping grid was placed on the CorvisST screen and the sensor and aperture opening were respectively aligned according to the measurement point on the grid. At each measurement point on both maps, the CorvisST airflow was triggered and recorded ten times consecutively, and the mean was used to obtain the pressure value at the specific point.

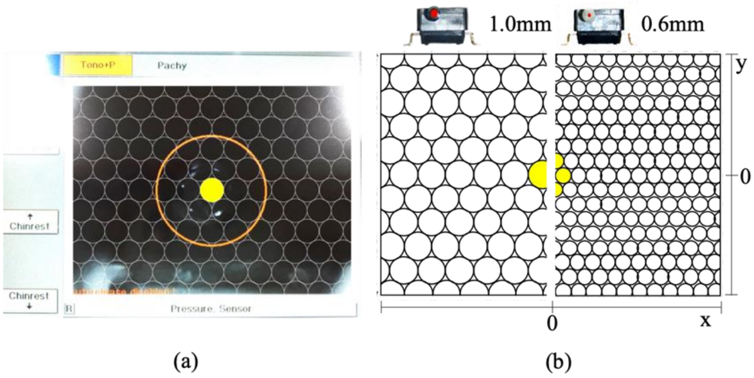

Figure 2: The spatial distribution of the CorvisST airflow pressure was investigated using mapping grids (a) which were based on the dimension of the CorvisST screen capturing the sensor tube opening, (b) resulting in the development of two mapping grids with a resolution of 1mm (m=137 measurement points) and of 600µm (m=382 measurement points). Circles highlighted in yellow represents the image of the sensor tube opening on the CorvisST screen (a) and on the two mapping grids (b).

Unlike the CorvisST, the ORA does not have a viewing screen and the pressure sensor tube opening was manually aligned with the tonometer nozzle for distance (11mm), height and tilt. To avoid parallax errors, two digital cameras were placed parallel and perpendicular to the ORA nozzle thus capturing a view of the nozzle and the sensor tube. The cameras were connected to a computer allowing simultaneous viewing and control of the position of the pressure sensor in real-time. Since the ORA was kept in a static position (Figure 3a) the tonometer nozzle and the sensor tube were aligned (Figure 3b). To allow visual alignment between sensor and nozzle, the casing of the pressure sensor was marked horizontally on each side with a straight line to highlight the centre of the sensor (Figure 3b, 1). The real time camera images on a computer screen were used to fit a digital level (Ruler for Mac V.20.2) between the nozzle and the sensor casing lines to amend the position of the sensor tube to the ORA nozzle. To investigate the spatial and temporal distribution, the pressure sensor was moved horizontally and vertically in one-millimetre increments until a measurement area of (13.0 x 7.0)mm was assessed; hence, in this manner 117 measurement points were evaluated. At each point, the ORA airflow was initiated ten times using the demo puff mode, and the average was used as the value for each position.

Preprints (www.preprints.org) | NOT PEER-REVIEWED | Posted: 27 January 2021 doi:10.20944/preprints202101.0566.v1

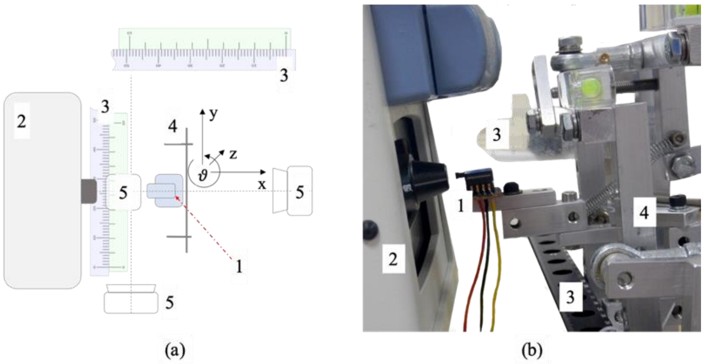

Figure 3: Set-up for the investigation of the ORA airflow a) schematically view from above and b) view from the side (1 pressure sensor, 2 ORA, 3 ruler, 4 movement apparatus, 5 camera).

2.2 Set up

The set-up required a digital oscilloscope (NI myDAQ) connected to a laptop (Toshiba LT, Intel Core i5-2520M CPU 2.5GH, RAM 8.00GB; Windows 7 Enterprise 64-bit). Both the pressure sensor and the mainboard of the CorvisST were connected to the oscilloscope. The sensor was housed in a custom designed holder which allowed precise horizontal, vertical and angular movement in 50µm increments. The distance between the nozzle and the sensor was adjusted to 11.0mm. To ensure adequate positioning spirit levels, digital rulers and two digital camera systems were used to line up the nozzle and the sensor position in real-time.

A programme was coded in LabVIEW 2015 (V15.0f2, 32-bit) to record and export pressure readings. The program was able to capture the different pressure input signals simultaneously (signals from both the sensor and CorvisST mainboard). The program consists of a loop (n=30) and the input signal range was set to 0 to 5V, 10 kHz and 20,000 samples. For each measurement, a time frame of 60 s and 1.2 million time points were recorded. Both output signals were saved as binary TDMS files containing the raw readings. Subsequently the binary TDMS files were imported into Microsoft Excel 2016 for Mac (Microsoft Inc., Redmond, Washington, USA). The maximum value of the piston-chamber pressure was used to synchronise the output signals. Airflow pressure and piston-chamber pressure data within ±30ms of the maximum piston-chamber pressure were extracted for further analysis.

For both devices conventional digital photo cameras were used to evaluate the position accuracy for the mapping procedure. One camera was positioned on axis with the sensor opening and the device nozzle, and one perpendicular, to capture the position of the sensor tube and nozzle for each measurement. Photos were then used to analyse the nozzle-sensor position accuracy for the horizontal and vertical distance as well as tilt.

Environmental factors such as the temperature, humidity and atmospheric pressure were monitored using a conventional hygrometer and a barometer app with GPS tracking and height calibration. Environmental variables such as temperature and humidity were kept constant throughout the experiment. To minimise the effects of background noise potentially contaminating sensor readings, data were collected over weekends or evenings after normal working hours.

2.3 Trigger signal

The piston chamber pressure is automatically recorded by the CorvisST and provided as a pressure reading (mmHg) per frame for each measurement. The main board signal to initiate the cylinder movement was used as a trigger to initiate the oscilloscope recording. In order to map the airflow pressure readings on to the CorvisST high-speed camera frame rate, the piston chamber pressure recorded by the LabView programme was synchronised with the CorvisST airflow pressure results. The LabView programme used to process the readings for the spatial and temporal assessment of the airflow provided a temporal resolution of 100µs whereas the CorvisST has a time resolution of 230.94µs (4330Hz) and hence to synchronise the two readings, the frequency recorded by the oscilloscope was reduced by 4330Hz for this purpose.

Unlike with the CorvisST, it was not possible to determine the location of the piston chamber pressure signal on the mainboard of the ORA. Therefore, the recorded airflow pressures were synchronised by their respective maximum value. This was challenging given that the ORA pressure values are only provided as a graphical output with discrete numbers per frame. Therefore, different frequencies were trialled to find the matching time domain resolution between the ORA and the oscilloscope output. These trials showed the recording frequency of the ORA's piston chamber pressure to be equivalent to 11kHz, which was used for further analysis.

3. Results

3.1 Evaluation of the experimental set up

3.1.1 Sensor noise and signal-to-noise ratio

The estimated type B uncertainty [29, 30] was found to be between 0.722 and 1.776kPa. Trial measurements for both devices showed that the recorded airflow pressure had maximal magnitudes of 1.600V (15.6kPa). Thus, the range of uncertainty for the airflow pressure was between 0.725 and 0.889kPa (5.433 to 6.669mmHg).

The average noise level of the sensor was detected to be 0.166kPa with a range from 0.139 to 0.168kPa (1.250mmHg from 1.041 to 1.258mmHg); airflow pressure less than the maximum noise level could be distinguished from the sensor noise.

The signal to noise ratio without applying an airflow was 48.4dB (V=0.185kPa, SD=0.70Pa) and was 17.6dB (V=1.445kPa, SD=191.20Pa) during the maximum airflow pressure. To minimise the noise of the sensor readings the raw data was smoothed by eliminating the Fourier components with higher frequencies than the calculated cut-off frequency using five consecutive data points as the analysis interval. This improved the signal to noise ratio, without applied pressure by 58.2dB (SD 0.226Pa) and during maximum airflow pressure by 57.0dB (SD 2.020Pa).

3.1.2 Mapping procedure

The position accuracy for the CorvisST was within ±0.03mm for the spatial assessment. The variability of the position of the tube opening and the ORA nozzle was ±0.44mm and included the inclination of the ORA nozzle.

3.2 CorvisST airflow pressure

3.2.1 Spatial distribution

The maximum pressure at the central measurement point was found to be (96.4 ± 1.42)mmHg (95%CI 96.1 to 96.6mmHg). The airflow pressure could be distinguished from the sensor noise within an area of 45.2mm^2. Within a radius of 3.8mm from the centre, the pressure had reduced by 20% to 80%, Figure 4a-c and Table 1. The airflow pressure was highly repeatable within the area affected (CoV 4.19%).

Preprints (www.preprints.org) | NOT PEER-REVIEWED | Posted: 27 January 2021 doi:10.20944/preprints202101.0566.v1

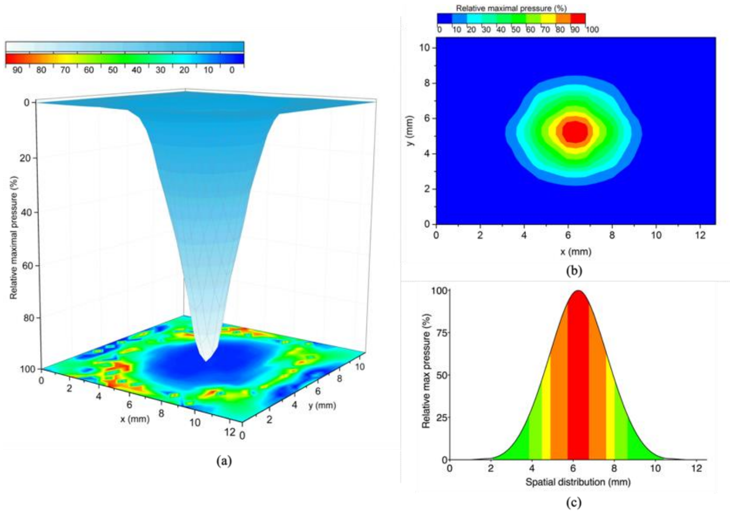

Figure 4: Spatial distribution of the maximum airflow pressure: a) 3D map of the spatial distribution. The bottom contour map shows the CoV of ten consecutive measurements at the respective locations. Low CoV is denoted by the blue colour, high CoV denoted by red. b) The relative pressure values were divided by the magnitude into ten intervals of pressure. With increasing distance from the centre, the pressure level reduced. c) The average spatial distribution profile highlights the different levels of pressures affecting the analysed area. The maximal airflow was detected centrally (red area).

Table 1: Spatial distribution of the relative airflow pressure in increments of 10%

Airflow pressure (%)	Area (mm^2)	Slope* (%/mm)	R^2
90-100%**	0.8	-	-
80-89%	1.9	-29.5	0.999
70-79%	3.5	-26.1	0.999
60-69%	5.7	-27.9	0.999
50-59%	7.5	-30.1	0.995
40-49%	10.2	-35.9	0.999
30-39%	13.8	-31.1	0.995
20-29%	20.4	-25.5	0.994
10-19%	45.2	-15.6	0.991

* Linear regression of the pressure relative to the maximum vs. the distance from the centre
** Peak radius of curvature 0.115mm

3.2.2 Temporal distribution

The duration of the airflow was (21.483 ± 0.2881)ms, (95%CI 21.427 to 21.539ms), whilst the maximum pressure plateau (defined as 99% quantile) lasted for (1.317 ± 0.1116)ms (95%CI: 1.295 to 1.339 ms), Figure 5a-b. For pressures greater than 25% of the maximum, the pressure duration was highly consistent with a CoV of less than 5%, Figure 5c. The time point when the respective maximum pressure was recorded was highly consistent across the affected area (CoV 1.3%), the time point varied by 0.3ms, Figure 5d.

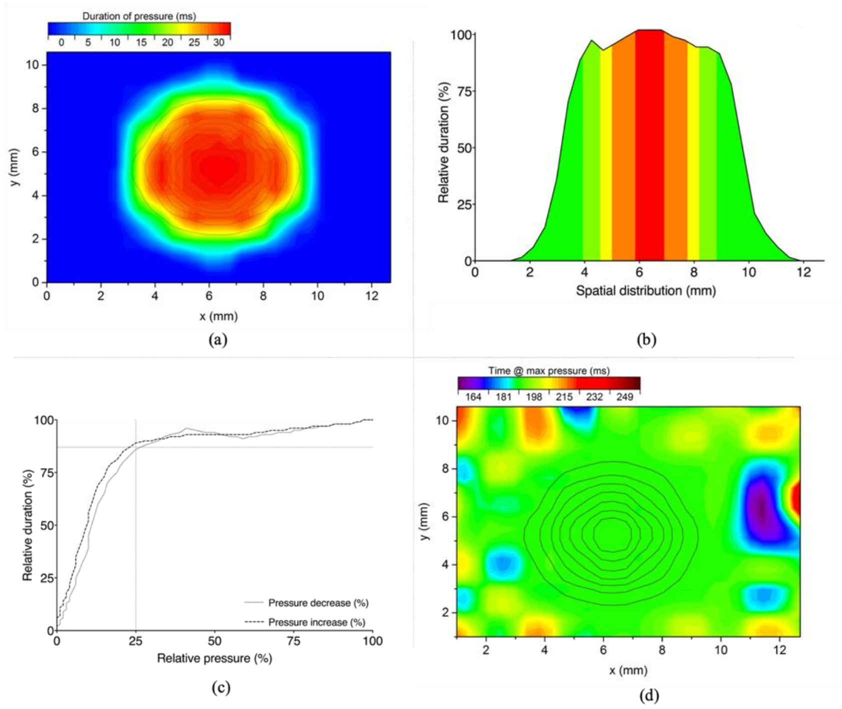

Figure 5: Time distribution of the maximum airflow pressure: a) Contour map shows the detected pressure duration. Short duration is denoted by the blue colour, long duration denoted by red. b) The average temporal distribution profile highlights the different levels of maximal pressure affecting the analysed area. The maximum airflow pressure was detected centrally (red area). c) The duration of pressures lower than 25% of the maximum where significantly shorter than the duration of higher pressures. d) The time point when the maximum pressure was detected was consistent within the area of the pressure (within the black contour lines which represent the ten pressure levels).

3.2.3 Airflow profile at the object plane of the CorvisST Scheimpflug camera system

The maximum piston chamber pressure was detected at frame 70 measuring 182.86mmHg, corresponding to the midpoint of the CorvisST analysis time of 140 frames. The mean difference of the piston chamber pressures detected by the CorvisST and by the oscilloscope was 0.2%. The pressure readings at 11mm distance for the central horizontal plane on the measurement map {x;y=0} was used to match the CorvisST time frame to allow comparison between the readings provided from the piston chamber and the pressure values recorded by the sensor, Figure 6. The airflow pressure extended to 7.2mm along the x-axis; 90% of the maximum pressure was found to have a horizontal diameter of 1.2mm. The sensor detected the maximum pressure at frame 65and the airflow could be distinguished from the sensor noise for 93 frames Figure 7a-c and Table 2.

 doi:10.20944/preprints202101.0566.v1

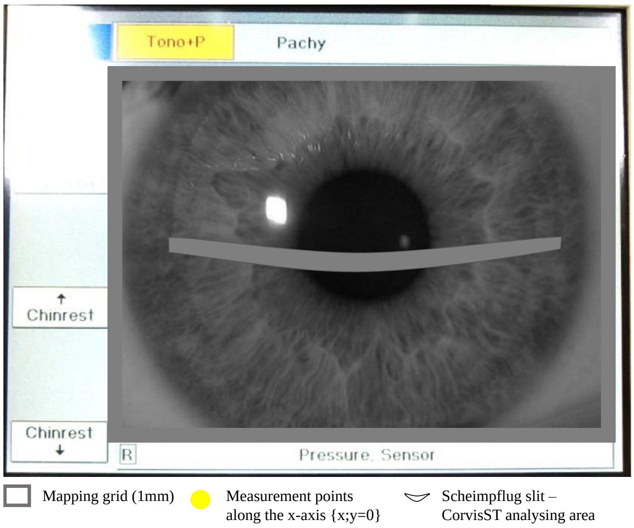

Figure 6: Schematic of the CorvisST screen highlighting the measurement area of the Scheimpflug imaging system and the horizontal measurement plane {x;y=0} on the measurement grid used to allocate the airflow pressure to the high-speed camera frame rate.

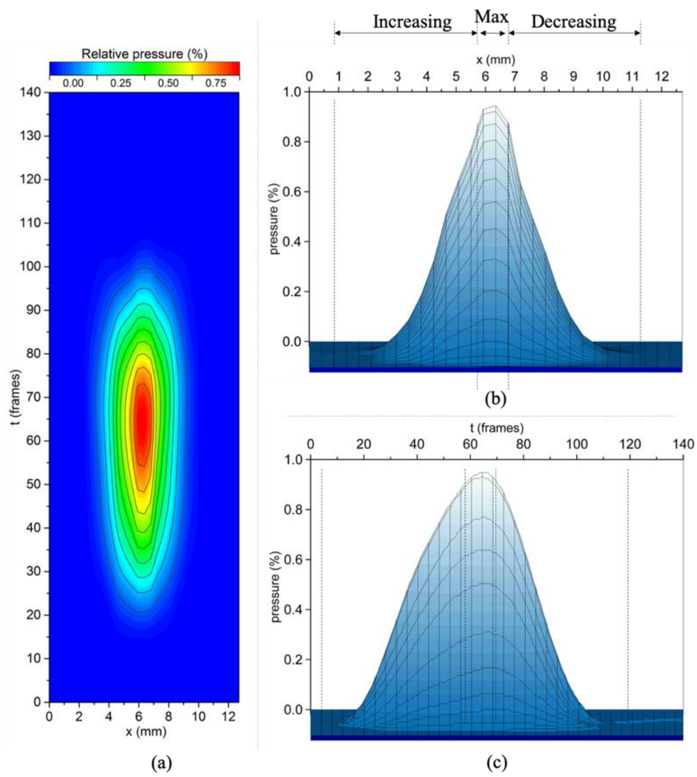

Figure 7: Relative airflow pressure at the central horizontal plane (a) 2D profile of the spatial and temporal distribution, which was separated (b) across the central horizontal plane (spatial distribution) and (c) over time (temporal distribution).

3.3 ORA airflow pressure

The ORA measurements are automatically provided within a frame range of 400 frames. The maximum of the provided discrete piston chamber pressure was reached on average after 42.5% of the measurement period (between frame 168 and 172; 15.288 and 15.652ms). Using a frequency of 11kHz the ORA analysing time period was equivalent to 36.360ms.

Preprints (www.preprints.org) | NOT PEER-REVIEWED | Posted: 27 January 2021 doi:10.20944/preprints202101.0566.v1

The maximum airflow pressure of the ORA was (91.7 ± 0.72)mmHg (95%CI 91.2 to 92.1mmHg) with a duration of (23.061 ± 0.1872)ms (95%CI 22.285 to 24.438ms) applied to an area of 35mm², Figure 8a-c. The maximum pressure, defined as 99% quantile lasted for (1.182 ± 0.1659)ms (95% CI 1.149 to 1.212ms).

The pressure decreased by 39.8% per millimetre distance from the centre towards the peripheral edges of the airflow. Within a diameter of 2.5mm around the maximum, the pressure reduced by 80% of the maximum, Figure 8a-c.

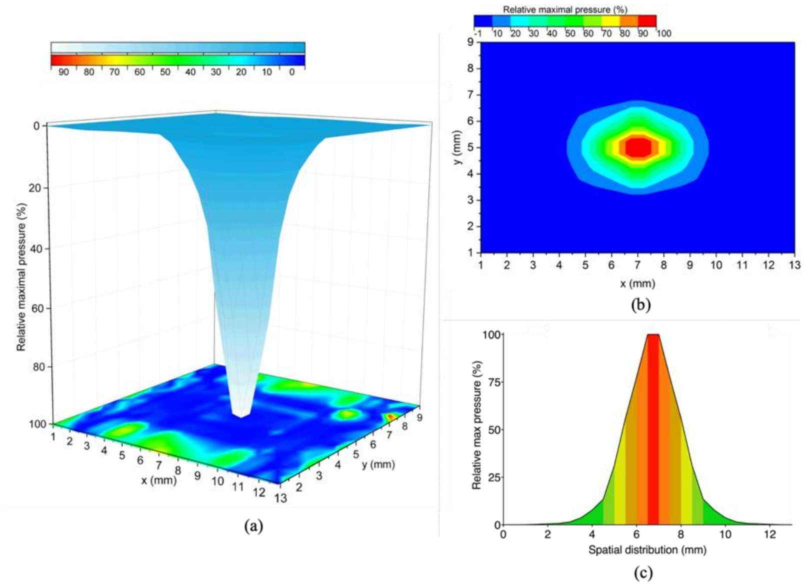

Figure 8: Spatial distribution of the ORA maximal airflow pressure (n=10): a) 3D map of the spatial distribution. The bottom contour map shows the CoV of ten consecutive measurements at the respective points. Low CoV is denoted by the blue colour, high CoV denoted by red. b) The relative pressure values were divided into deciles. The maximum pressure (90 to 100%) was detected centrally in an area of 1mm². c) The average spatial distribution profile highlights the different levels of pressures affecting the analysed area.

Table 2: Temporal distribution of the relative airflow pressure at the central horizontal plane at 11mm distance

Phase*		Airflow pressure (%)	Duration (frames)	Slope (%)	R^2
Pressure free		0.01 to 0.09	8 (1-9)	> 0.000	0.949
(1) Increasing	Slow	0.09 to 4.52	8 (10-18)	0.70	0.928
	Sharp	5.80 to 98.14	42 (19-61)	2.39	0.988
Maximum		99.51 ± 0.456	6 (62-68)	< 0.000	0.002
(2) Decreasing	Sharp	98.89 to 5.54	31 (69-100)	-3.13	0.995
	Slow	4.37 to 0.22	8 (101-109)	-0.96	0.973
Pressure free		0.22 to 0.00	30 (110-140)	> 0.000	0.974

* 2nd derivate of the graphical analysis of time distribution was used to distinguish between the different phases

3.4 Regression modelling

The maximum airflow pressures changed over time while the cross-section was approximately constant for both devices. The spatial and temporal distribution of the airflow pressures could be described by a Gaussian function, Equation (1) and **Error! Reference source not found.**. The curves fitted to the airflow pressure of both the CorvisST and ORA did not follow a normal distribution ($p<0.050$). Comparing the two main meridians of the spatial distribution ($t = t[p_{max}]$) across the horizontal $p(x)$ and vertical $p(y)$ meridians for

Preprints (www.preprints.org) | NOT PEER-REVIEWED | Posted: 27 January 2021 doi:10.20944/preprints202101.0566.v1

both devices show minor differences relative to the average pressure at the respective measurement location:

- CorvisST $\Delta p(p_x - p_y) = (0.6 \pm 0.45)\%$ and
- ORA $\Delta p(p_x - p_y) = (-0.4 \pm 1.19)\%$.

Thus, both airflows can be considered as rotationally symmetrical.

$$P_{airflow}(t,a) = P_{max}(t) \cdot e^{-2 \cdot \frac{(a-a_{max})}{w_a^2}} \quad (1)$$

$p_{airflow}$ = Airflow pressure (mmHg)
t = time (ms)
p_{max} = Maximum airflow pressure (mmHg)
w = Width (unit of a)

3.5 Comparison between the central CorvisST and ORA airflow pressures

The ORA airflow measurement commenced at 0.693ms and lasted for 23.061ms; 2.5% longer than the CorvisST airflow. The maximum airflow pressure for the ORA was reached 1.155ms before the CorvisST maximum and it was 4.9% lower and more curved (skewness: CorvisST 0.549, ORA 0.657, kurtosis: CorvisST -1.322, ORA -1.113). The duration of the maximum pressure was shorter with the ORA (1.182 ± 0.1659)ms when compared to the CorvisST (1.317 ± 0.1116)ms. The mean difference between the CorvisST and ORA airflow pressures was (2.6 ± 4.07)mmHg (95%CI from -5.5 to 10.6mmHg), Figure 9.

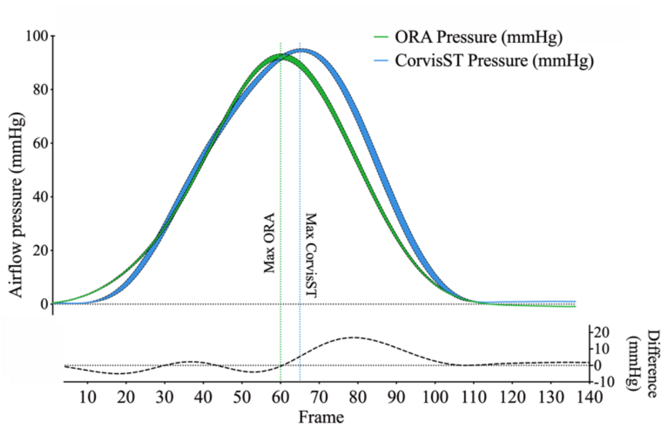

Figure 9: Graphical analysis of comparison between the CorvisST (blue) and ORA (green) airflow pressure over time with the respective 95%CI error bands (n=10). The time of respective maximum is highlighted (vertical dotted lines). The differences (CorvisST -ORA) are shown in the diagram below.

4. Discussion

Understanding the fundamental physical characteristics of the airflow pressures produced by non-contact tonometers is vital when interpreting measures of intraocular pressure and corneal biomechanics. The present study reports on the development of a robust methodology to investigate the temporal and spatial characteristics of the air pressure produced by non-contact tonometers.

4.1 CorvisST airflow pressure

In comparison to previous studies [20-23], the maximum pressure produced by the CorvisST was lower in regards to both magnitude of pressure and duration. In regard to the temporal profile, the values suggest a sharper change than suggested previously. Significant differences in the procedures and components used between studies are likely to contribute to the variation in results observed in the literature. Kling et al. [22] also used a piezoresistive pressure sensor to investigate the airflow pressure. The preliminary

Preprints (www.preprints.org) | NOT PEER-REVIEWED | Posted: 27 January 2021 doi:10.20944/preprints202101.0566.v1

investigation into the variability of the sensors revealed that peripheral air streams around the differential pressure sensor tube opening had a significant influence on the measured value, leading to an overestimation of the recorded value. [22]

Metzler et al. [20, 23] used a hot wire anemometer to assess the airflow velocity. However, the tenability of relating airflow velocities to pressure values is not comparable to this study given that the wire of the hot-wire anemometer is placed perpendicular to the airflow direction: Integration of measurements across the wire length (1-3mm) can lead to an overestimation of the maximal stagnation pressure.

Numerical simulations are limited by the assumptions used during modelling. As such, in their simulation model, Bahr et al. [21] assumed the velocity at the nozzle to be 80m/s, e.g. the dynamic stagnation pressure of the airflow was 52.1mmHg. It may be that the investigators used the values published by Grolman [19] describing the prototype of the non-contact tonometer, with an airflow velocity within the range of 83.3 to 111.1m/s. The values reported by Grolman [19] appear to be underestimated as shown by Metzler et al. [20], Kling et al. [22]; the present study found the velocity of the airflow at the nozzle to be much higher by over 100m/s [20], 115m/s [22] and 99.5m/s in the present study. Using a smaller value leads to an underestimation of the pressure applied to the cornea.

4.2 ORA airflow pressure

Little is known of the temporal and spatial characteristics of the ORA airflow. Using a fast response pressure sensor with a micro-aperture and an opening of 0.25 mm, Luce [24] investigated the vertical and horizontal spatial pressure profile of the ORA. Regarding the spatial extent of the airflow, 50% of the maximum airflow was found to be within 2.9 mm with a high CoV of 3%. Furthermore, the repeatability of the absolute airflow pressure within the central 3mm zone was high (CoV 5%). In a separate study the duration of the airflow was reported to be approximately 20ms, with a symmetrical profile for increase and decrease edges. [2] The findings in the present study are in concordance with Luce's observations.

4.3 Comparison between the airflow pressures of the CorvisST and ORA

It is evident that there are differences in the temporal and spatial distribution of the CorvisST and ORA airflow pressure. The most distinctive differences were the maximal pressure at 11 mm distance, the pressure change during the increasing phase and the area affected. In total, the CorvisST airflow is stronger, shorter and of a higher magnitude than that of the ORA.

4.4 Limitations

As discussed previously, the pressure sensor used had an input depended on the measurement uncertainty. Due to the sensor noise, the maximum airflow pressures varied in the range of the uncertainty. To reduce the influence of the measurement uncertainty for each airflow pressure value, at least ten consecutive measurements were conducted and averaged. The novel measurement procedure described in this study had two main sources of random errors: the electrical components, sensor and digital oscilloscope, and the procedure to obtain spatially and distance distribution of the respective airflow. In order to minimise the random errors, the detected signal has undergone a smoothing procedure and the relative nozzle to sensor position was controlled by using real-time monitoring and capturing the position for each measurement. Additionally, environmental conditions like temperature, humidity and noise level were kept as stable as possible. A systematic error of the measurement procedure was not detected.

5. Conclusions

For accurate interpretation of the clinical measurements produced by the CST and ORA and allowing meaningful comparison of results between devices a thorough understanding of the spatial and temporal characteristics of the tonometers' airflow is vital. Using a high precision sensor and recording system for measuring low-level pressure of short duration the study presents novel data on the dimension, magnitude and duration of the airflow pressure generated by these devices. With the use of a custom designed mapping system the investigation provides an insight into the size of the area affected during application of the pressure as well as its repeatability. In comparison to the ORA, CorvisST airflow was found to impact on a larger corneal area with greater strength and shorter duration. It is anticipated that the methodologies presented herein may provide a systematic means of assessing the tonometer airflow with the cornea which is essential to develop an analytical model to describe the changes in the viscoelastic properties of the cornea.

Author Contributions: DO designed and performed the experiments, derived the models, analysed the data and took lead in writing the manuscript. DJ supported the experimental set up and gave initial ideas to the sensor selection; PB, HB supervised the project and reviewed the manuscript. All authors gave final approval for publication and agree to be held accountable for the work performed therein.

Funding: This work was supported by the University of Plymouth and a College of Optometrist Fellowship for HB.

Data Availability Statement: The data presented in this study are available on request from the corresponding author.

Acknowledgments: Julie Soane, who always supported the work and had the most excellent ideas, independent on the matter. Paul Davey who provided his expertise to initially set up the experiment and made PD and DO meet.

Conflicts of Interest: The authors declare no conflict of interest.

References

1. Hon, Y. and A.K. Lam, *Corneal deformation measurement using Scheimpflug noncontact tonometry.* Optom Vis Sci, 2013. **90**(1): p. e1-8.
2. Luce, D.A., Determining in vivo biomechanical properties of the cornea with an ocular response analyzer. J Cataract Refract Surg, 2005. 31(1): p. 156-62.
3. Vantomme, M., S. Pourjavan, and M. Detry-Morel, The range of the waveform score of the ocular response analyzer (ora) in healthy subjects. Bull Soc Belge Ophtalmol, 2013(322): p. 91-7.
4. Luce, D. and D. Taylor, Reichert Ocular Response Analyzer measures corneal biomechanical properties and IOP - Provides new indicators for corneal specialties and glaucoma management. Reichert Ophthalmic Instruments, 2006.
5. Luce, D., Methodology for cornea compensated IOP and corneal resistance factor for the Reichert Ocular Response Analyzer, in Investigative Ophthalmology & Visual Science. 2006. p. 2266-2266.
6. Zhao, Y., et al., Relationship among corneal stiffness, thickness, and biomechanical parameters measured by Corvis ST, Pentacam and ORA in keratoconus. Frontiers in Physiology, 2019.
7. Wu, W., R. Dou, and Y. Wang, Comparisons of the corneal biomechanics between low and high myopic eyes–a meta-analysis. American Journal of Ophthalmology, 2019.
8. Wang, L., et al., Corneal Biomechanical Properties Characterization Using Air-jet Indentation Based Optical Coherence Tomography System (AIOCT). MATEC Web of …, 2019.
9. Wallace, H., et al., Biomechanical changes in the cornea following cataract surgery: A prospective assessment with the Corneal Visualisation Scheimpflug Technology. Clinical & experimental …, 2019.
10. Wallace, H., et al., Corneal Curvature: the Influence of Corneal Accommodation and Biomechanics on Corneal Shape. … Vision Science & …. 2019: iovs.arvojournals.org.
11. Vinciguerra, R., et al., Assessment of the association between in vivo corneal biomechanical changes after corneal cross-linking and depth of demarcation line. Journal of Refractive …, 2019.
12. Hon, Y. and A. Lam, Corneal deformation measurement using Scheimpflug noncontact tonometry. Optometry and Vision Science, 2013.

13. Laiquzzaman, M., et al., Diurnal variation of ocular hysteresis in normal subjects: relevance in clinical context. Clin Experiment Ophthalmol, 2006. 34(2): p. 114-8.
14. Shah, S., et al., The use of the Reichert ocular response analyser to establish the relationship between ocular hysteresis, corneal resistance factor and central corneal thickness in normal eyes. Contact lens and Anterior eye, 2006. 29(5): p. 257-262.
15. Shah, S., et al., Ocular response analyser to assess hysteresis and corneal resistance factor in low tension, open angle glaucoma and ocular hypertension. Clinical & experimental …, 2008.
16. Wolffsohn, J.S., et al., Changes of corneal biomechanics with keratoconus. Cornea, 2012. 31(8): p. 849-54.
17. Bergmann, L., et al., Lehrbuch der Experimentalphysik 5. Gase, Nanosysteme, Flüssigkeiten. 2005: de Gruyter.
18. Fatt, I. and B.A. Weissman, Physiology of the Eye: An Introduction to the Vegetative Functions. 2013: Elsevier Science.
19. Grolman, B., A new tonometer system. Am J Optom Arch Am Acad Optom, 1972. 49(8): p. 646-60.
20. Metzler, K., et al., The Influence of IOP, Corneal Stiffness, and Sclera on Corneal Deformation Response to an Air Puff Using the CorVis ST, in Biomedical Engineering. 2013, The Ohio State University: Investigative Ophthalmology & Visual Science. p. 62.
21. Bahr, N., et al., Modelling the Deformation of the Human Cornea Produced by a Focussed Air Pulse. Computational Biomechanics for Medicine, 2015: p. 93-100.
22. Kling, S., et al., Corneal viscoelastic properties from finite-element analysis of in vivo air-puff deformation. PLoS One, 2014. 9(8): p. e104904.
23. Metzler, K., et al. Modeling corneal response to an air puff using deformation data to derive Young's modulus. in ARVO. 2013. Investigative Ophthalmology & Visual Science.
24. Luce, D., Air–Jet Temporal and Spatial Pressure Properties of the Reichert Ocular Response Analyzer (ORA). Investigative Ophthalmology & Visual Science, 2005. 46(13): p. 5009-5009.
25. Asaoka, R., et al., The Relationship between Corvis ST Tonometry Measured Corneal Parameters and Intraocular Pressure, Corneal Thickness and Corneal Curvature. PLoS One, 2015. 10(10): p. e0140385.
26. Haustein, M., E. Spoerl, and L. Pillunat, Correlation of Biomechanic Parameters Measured by Corvis ST (Oculus®) and by Ocular Response Analyzer (ORA, Reichert®). Investigative Ophthalmology & Visual Science, 2013. 54(15): p. 1626-1626.
27. Matsuura, M., et al., The Relationship between Corvis ST Tonometry and Ocular Response Analyzer Measurements in Eyes with Glaucoma. PLoS One, 2016. 11(8): p. e0161742.
28. Tejwani, S., et al., Biomechanics of the cornea evaluated by spectral analysis of waveforms from ocular response analyzer and Corvis-ST. PLoS One, 2014. 9(8): p. e97591.
29. Taylor, B.N. and C.E. Kuyatt, Guidelines for evaluating and expressing the uncertainty of NIST measurement results. 1994: US Department of Commerce, Technology Administration, National Institute of Standards and Technology Gaithersburg, MD.
30. Hässelbarth, W., BAM-Leitfaden zur Ermittlung von Messunsicherheiten bei quantitativen Prüfergebnissen-1. Fassung März 2004. 2004.